Climate Network Analysis of Precipitation Regimes from WorldClim Data in Saudi Arabia

Yazeed Alabbad[1*], Ali Alnahit[1], Saleh Alhathloul[1]

[1] Department of Civil Engineering, College of Engineering, King Saud University, P.O. Box 800, Riyadh, 11421, Saudi Arabia

[*] Corresponding Author, Email: yalabbad@ksu.edu.sa,

Abstract

Saudi Arabia is shaped by a hydroclimatic gradient, from the hyper-arid Rub' al-Khali desert to the semi-arid mountains in the southwest. This gradient affects runoff generation, groundwater recharge, and drought risk, yet most studies still summarize rainfall using basic statistics from station data or gridded products. This research applies climate network analysis to identify coherent rainfall regimes across Saudi Arabia. Monthly precipitation climatology (1970-2000) from WorldClim v2.1 at 2.5 arc-minute resolution was extracted for 98,719 land grid cells. Cells were assigned to three macro-zones based on annual precipitation: hyper-arid (less than 75 mm), arid (75-150 mm), and semi-arid (150 mm or more). A stratified sampling scheme selected 7,148 representative nodes while preserving the distribution of annual rainfall. Within each zone, we constructed climate networks by linking nodes with highly similar seasonal cycles. We then computed standard network metrics (degree centrality, betweenness centrality) and identified communities through a modularity-based algorithm. The zonation reproduces the precipitation gradient, and the sampling design captures the range of annual totals. In each zone networks exhibit dense connectivity and two or three communities that align with seasonal regimes and topographic settings. Nodes with high degree centrality mark areas where the seasonal cycle is typical of their zone, whereas nodes with elevated betweenness centrality occur along transition belts and coastal margins that connect distinct regimes. Sensitivity tests across correlation thresholds show that community patterns are robust even as network density and centrality values decline. By converting rainfall data into a network structure, this study provides a framework to describe spatial rainfall behavior. The framework offers practical value for hydrological analysis, water-resource planning, and flood and drought preparedness.

Keywords: Climate network, Precipitation, Rainfall, Arid regions, Hydroclimatic regionalization

1. Introduction

Precipitation in arid and semi-arid regions is shaped by an interplay of large-scale circulation, regional topography, and local convective processes (Almazroui et al., 2012; Nelli et al., 2021). Over the Arabian Peninsula, this interplay creates strong gradients between the hyper-arid Rub' al Khali (Empty Quarter desert), the arid interior plateau, and the orographic southwestern mountains. Station and satellite-based studies show that annual rainfall totals increase from the interior deserts toward the Asir and Hijaz ranges and parts of the Red Sea coastal zone, while much of central and eastern Saudi Arabia receives less than 100 mm annually and the Rub' al Khali is almost rain-free (Abdullah & Al-Mazroui, 1998; Bahrawi, 2018; Hasanean & Almazroui, 2015). Seasonal analyses further indicate that southwest of the country experiences rainfall in most seasons with a spring maximum, whereas summer and winter precipitation in the north and interior is weaker and more episodic (Almazroui & Hasanean, 2020; Hasanean & Almazroui, 2015). These spatial and seasonal contrasts have direct implications for groundwater recharge, flash-flood risk in steep wadis, and the design of water supply systems in rapidly growing cities.

A substantial body of work has examined rainfall climatology and variability over Saudi Arabia using gauge networks, satellite products, and regional climate models. Early regionalization and station-based analyses documented the structure of the southwestern rainfall maximum and its relationships to elevation and orography (Abdullah & Al-Mazroui, 1998; Hasanean & Almazroui, 2015). Subsequent studies calibrated and evaluated satellite products such as Tropical Rainfall Measuring Mission (TRMM) over the Kingdom, showing that uncorrected satellite climatologies can be biased and require careful adjustment against in situ observations (Almazroui, 2011; Bahrawi, 2018). More recent work has assessed the performance of CMIP5 and regional climate simulations for Saudi Arabia and the wider Arabian Peninsula, highlighting robust warming and regionally important but uncertain changes in precipitation and extremes (Almazroui et al., 2017; Almazroui, 2019). Together, these studies provide a detailed description of mean rainfall and its trends, but they mostly treat each grid cell or station independently and seldom ask how different parts of the country are linked through shared precipitation regimes.

In data-scarce environments, gridded climatological products offer a complementary way to map spatial patterns of climate. The WorldClim v2.1 data set provides monthly climate normals for 1970–2000 at 2.5 arc-minute resolution, derived from weather stations and elevation-based interpolation, and has become a standard input for ecological, hydrological, and climate-impact modelling (Cerasoli et al., 2022; Fick & Hijmans, 2017). For precipitation, WorldClim reproduces large-scale gradients but tends to smooth sharp orographic contrasts, especially where station density is low and rainfall is highly variable in time and space (Cerasoli et al., 2022; Fick & Hijmans, 2017). Despite these limitations, such products provide contiguous coverage over Saudi Arabia and are therefore attractive for methods that require a spatially consistent field rather than isolated station time series. However, most applications still reduce these data to

simple maps of mean annual rainfall or bioclimatic indices, which only partially capture the structure of rainfall regimes.

Complex network theory offers a different perspective by representing climate fields as graphs (networks), where nodes correspond to spatial locations and links represent statistical similarity in their temporal behavior (Alabbad et al., 2022; Zou et al., 2019). Early work showed that correlation networks derived from atmospheric fields such as geopotential height and surface temperature contain hubs (highly connected nodes) and communities (clusters of nodes) that coincide with known teleconnection patterns and circulation regimes (Tsonis & Roebber, 2004; Yamasaki et al., 2008). Methodological studies have compared linear and nonlinear similarity measures, examined the backbone structure of climate networks, and discussed interpretations of metrics such as degree, betweenness centrality, and modularity can be interpreted in terms of dynamical pathways and dominant variability modes (Donges et al., 2009a, 2009b; Marwan et al., 2009; Steinhaeuser et al., 2009; Zou et al., 2019). However, recent work has emphasized that choices in network construction, including correlation thresholds and significance testing, strongly influence the resulting topology and must be considered carefully (Haas et al., 2023).

Precipitation-based climate networks have been developed more recently and mostly at global or continental scales. Networks built from global precipitation fields reveal that regions such as the Sahel and eastern Australia act as highly connected, reflecting relatively homogeneous rainfall fields, whereas monsoon regions often show shorter-range connectivity because of localized extremes (Scarsoglio et al., 2013; Wolf & Donner, 2021). Studies focusing on extreme rainfall events in the South American Monsoon System and over the Indian subcontinent have used event synchrony or coincidence to identify coherent regions of extreme rainfall and their seasonal evolution (Boers et al., 2013; Stolbova et al., 2014; Wolf & Donner, 2021). More recently, high-resolution satellite products have been used to uncover global teleconnections of extreme rainfall, showing long-range coupling consistent with planetary wave patterns (Boers et al., 2019; Wolf & Donner, 2021). These studies demonstrate that network approaches can uncover spatial organization and teleconnections in precipitation that are difficult to infer from traditional correlation maps or regionalization techniques.

At the same time, most precipitation network studies have focused on extreme events, global teleconnections, or wet regions, and few have been applied to hyper-arid climates. A number of papers have analyzed rainfall trends, extremes, and circulation controls over the Arabian Peninsula, but these generally use conventional statistical or dynamical approaches rather than network-based diagnostics (Almazroui et al., 2017; Almazroui et al., 2019; Almazroui & Hasanean, 2020; Hasanean & Almazroui, 2015). To our knowledge, there has been no systematic attempt to treat Saudi Arabia as a set of interconnected precipitation nodes. Such an analysis is particularly relevant because the country's sparse rain gauge coverage and sharp spatial gradients make it difficult to extrapolate local observations.

In this study, precipitation climate networks were constructed for Saudi Arabia using WorldClim v2.1 long-term monthly precipitation normals at 2.5-arc-minute resolution for the period 1970-2000 (Fick & Hijmans, 2017). Grid cells are first grouped into three macro-zones based on annual rainfall totals, hyper-arid (less than 75 mm), arid (75–150 mm), and semi-arid (150 mm or more), reflecting the major hydro-climatic divisions identified in previous climatological work over the Kingdom (Abdullah & Al-Mazroui, 1998; Hasanean & Almazroui, 2015). A stratified sampling scheme is then used to select a manageable number of representative nodes from the full grid while preserving the distribution of annual precipitation across the country. Within each macro-zone, we construct undirected climate networks by linking nodes whose 12-month precipitation climatology vectors are highly correlated, and we compute degree centrality, betweenness centrality, and modularity-based communities to characterize the internal structure of each zone.

The objectives of this study aim to identify coherent rainfall communities within each annual precipitation zone and to examine how these communities relate to topography and known regional precipitation regimes, such as the southwestern orographic belt and the northern frontal zones (Abdullah & Al-Mazroui, 1998; Bahrawi, 2018). Also, we evaluate the sensitivity of network topology to the choice of correlation threshold, focusing on changes in edge density, centrality distributions, and the number of communities (Donges et al., 2009a; Haas et al., 2023). This research offers a reproducible workflow for applying climate network analysis to gridded precipitation climatologies in data-scarce arid regions, highlighting its strengths, limitations, and potential to complement traditional rainfall maps in hydrologic, agricultural, and hazard-planning contexts. This framework provides a clearer structural understanding of rainfall patterns across Saudi Arabia and supports more informed hydrologic and climate-related decision making. It also helps water-resource practitioners improve modeling approaches and enhance the reliability of their results.

2. Methodology

2.1. Case Study

The study covers mainland Saudi Arabia, which extends from approximately 16° to 32° N and from 34° to 56° E (Figure 1). The terrain is dominated by the Arabian Shield and western escarpment, the central Najd plateau, and the vast Rub' al Khali desert in the southeast. Elevation of the study area at 2.5 arc-minute resolution extracted from WorldClim ranges from near sea level along the Red Sea and Arabian Gulf coasts to more than 2500 m in the southwestern highlands. These physiographic contrasts strongly influence the spatial distribution of precipitation.

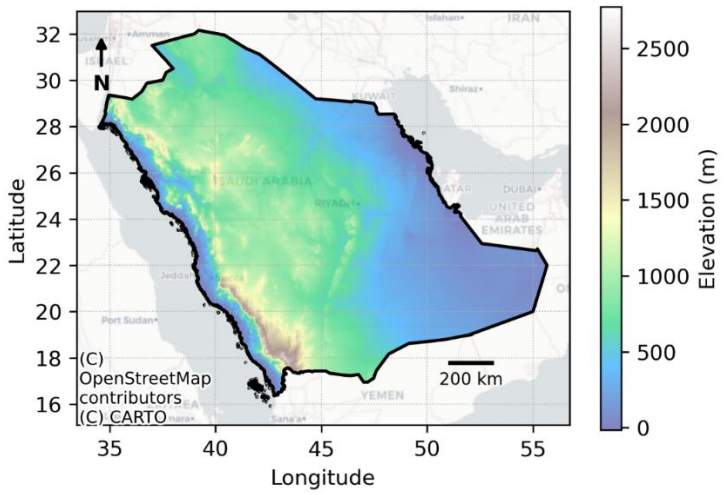

Figure 1. Map of Saudi Arabia showing the study area boundaries and elevation distribution.

2.2. WorldClim Precipitation Data

We used monthly precipitation climatology from the WorldClim v2.1 data set at 2.5 arc-minute resolution (approximately 5 km near the equator). WorldClim provides long-term average climate surfaces for the period 1970-2000, derived from quality-controlled station records and covariates such as elevation, and interpolated using thin-plate splines (Fick & Hijmans, 2017). These data are widely used in eco-hydrological and climate-impact assessments because they offer homogeneous global coverage in regions with sparse gauge networks (e.g., Lutz et al., 2016; Zomer et al., 2008; Mankin et al., 2025; Jahn et al, 2025). The subset covering Saudi Arabia contains 98,719 land grid cells with 12 monthly precipitation values, which we denote $P_i^{(m)}$ for month $m = 1, \ldots, 12$ at grid cell i. For each grid cell, annual precipitation was computed as the sum of the twelve-monthly values:

$$P_{\text{ann}}(i) = \sum_{m=1}^{12} P_i^{(m)} \qquad (1)$$

This annual total was used both for defining precipitation zones and for the stratified sampling scheme that selects network nodes.

2.2.1. Annual Precipitation-based Zoning

To avoid mixing fundamentally different rainfall regimes within a single network, we partitioned the domain into three broad precipitation zones using annual precipitation These are consistent with international classifications of hyper-arid, arid, and semi-arid climates (Gratzfeld, 2003; Middleton & Thomas, 1997; UNEP, 1997). Hyper-arid regions are typically defined by very low annual precipitation or low aridity index values, while arid and semi-arid regions receive higher

totals but remain water-limited (UNEP, 1997; Dastorani & Poormohammadi, 2016). Saudi Arabia spans this continuum from hyper-arid deserts in the Rubʿ al Khali to semi-arid orographic zones along the southwestern escarpment (Almazroui et al., 2012; Hereher, 2016).

Let $P_{\text{ann}}(i)$ be the annual precipitation at cell i. We define

$$\text{Zone}_i = \begin{cases} 1, & P_{\text{ann}}(i) < 75 \text{ mm (hyber-arid)} \\ 2, & 75 \le P_{\text{ann}}(i) < 150 \text{ mm (arid)} \\ 3, & P_{\text{ann}}(i) \ge 150 \text{ mm (semi-arid)} \end{cases} \qquad (2)$$

These thresholds are not based on a strict aridity index, but they align with common distinctions: hyper-arid zones typically receive less than 100 mm, while arid and semi-arid zones range up to 300 mm and beyond (Gratzfeld, 2003; UNEP, 1997; Dastorani & Poormohammadi, 2016). They also reflect the strong spatial gradient from the Rubʿ al Khali to the Asir highlands (Almazroui et al., 2011; Hereher, 2016). Applying this classification yields 30,647 cells in Zone 1, 51,662 in Zone 2, and 16,410 in Zone 3.

2.2.2. Stratified sampling of network nodes

Constructing a full correlation network on almost 100,000 nodes is computationally expensive and makes both community detection and visualization cumbersome, especially when centrality measures need to be evaluated repeatedly for sensitivity tests (Donges et al., 2009a; Newman, 2010). At the same time, simple random subsampling could under-represent rare but important rainfall regimes, such as the wettest mountain cells. To balance representativeness and feasibility, we designed a stratified sampling scheme based on annual precipitation, which is a standard approach for preserving the marginal distribution of a key variable in survey sampling and environmental monitoring (Lohr, 2021; Cochran, 1977).

We first divided the range of P_i^{ann}over the study area into B non-overlapping bins:

$$B_b = \left(P_b^{\min}, P_b^{\max}\right], \qquad b = 1, \dots, B \qquad (3)$$

In this study we used $B = 8$ bins chosen to cover the observed annual rainfall range (4-299 mm), with narrower bins in the most densely populated parts of the histogram so that both dry and wet regimes are well represented. For each bin B_b we randomly sampled up to n_b grid cells without replacement, with a target of $n_b = 1000$ nodes per bin when sufficient cells were available. The total sample size is 7,148 nodes.

Because sampling is conditioned on annual rainfall, the sample reproduces the full rainfall histogram of the WorldClim grid and covers all three climatic zones. Within the sample, approximately 27 %, 29 %, and 44 % of nodes fall in Zones 1, 2, and 3 respectively, which intentionally give greater weight to the rarer wet areas (Zone 3) compared to their raw occurrence

(17% in full grid), while still sampling plenty of dry and arid points. This design reduces computational cost while preserving the diversity of rainfall regimes that are needed for a meaningful climate network analysis.

2.3. Network Construction

For each precipitation zone we constructed an undirected, unweighted climate network based on the similarity of monthly precipitation at the sampled grid cells. This follows the standard correlation based approach that has been widely used to study connectivity and teleconnections in climate fields such as temperature, geopotential height and precipitation (Donges et al., 2009a; Tsonis & Roebber, 2004; Deza & Deza, 2009). All calculations were implemented in Python using the libraries NumPy for numerical operations, pandas and GeoPandas for tabular and spatial data handling, and NetworkX for graph construction and centrality metrics (Hagberg et al., 2008).

2.3.1. Similarity Metric: Pearson correlation

Within each zone, every sampled grid cell i has an associated 12-element vector of monthly precipitation climatology

$$\mathrm{P}_i = (P_i^{(1)}, P_i^{(2)}, \dots, P_i^{(12)}) \quad (4)$$

where $P_i^{(m)}$is the mean precipitation in month m during 1970–2000 at cell i. For two nodes i and j in the same zone, we quantify the similarity of their seasonal cycles using the Pearson product–moment correlation coefficient (Equation 5)

$$r_{ij} = \frac{\sum_{m=1}^{12} (P_i^{(m)} - \bar{P}_i)\,(P_j^{(m)} - \bar{P}_j)}{\sqrt{\sum_{m=1}^{12} (P_i^{(m)} - \bar{P}_i)^2}\,\sqrt{\sum_{m=1}^{12} (P_j^{(m)} - \bar{P}_j)^2}} \quad (5)$$

where $\bar{P}_i$ and $\bar{P}_j$ are the mean monthly precipitation values at nodes i and j. Pearson correlation is widely used in climate network studies because it is scale independent, easy to interpret, and highlights similarity in the shape of the annual cycle rather than only the absolute magnitude of rainfall (Donges et al., 2009a; Deza & Deza, 2009). For each zone we use NumPy to assemble the full correlation matrix R, with entries $R_{ij} = r_{ij}$.

2.3.2. Thresholding and adjacency matrix

To obtain a sparse network that emphasizes strong statistical links, we apply a correlation threshold r_{thr}. The binary adjacency matrix A is defined as

$$A_{ij} = \begin{cases} 1, & i \neq j \text{ and } r_{ij} > r_{\text{thr}}, \\ 0, & \text{otherwise}, \end{cases} \qquad (6)$$

with the diagonal set to zero in order to avoid self-loops. The resulting graph $G = (N, E)$ has N nodes (sampled grid cells) and E undirected edges, where

$$E = \frac{1}{2} \sum_{i=1}^{N} \sum_{j=1}^{N} A_{ij} \qquad (7)$$

The choice of r_{thr} influences the number of edges, the distribution of centrality values and, potentially, the detected communities (Haas et al., 2023). To assess robustness, we perform a sensitivity analysis using three thresholds, $r_{\text{thr}} = 0.75, 0.80, \text{and } 0.85$. This range is consistent with previous correlation based climate network studies that focus on strong, statistically meaningful links rather than weak background correlations (Donges et al., 2009a; Tsonis & Roebber, 2004; Deza & Deza, 2009). We choose an intermediate value (r_{thr} = 0.80) as the reference for our main analysis, and also assess two bracketing values (0.75, 0.85) for sensitivity. For each threshold and each zone, we use NetworkX to build the graph from A and to compute degree centrality, betweenness centrality and modularity based communities, which are analysed in the subsequent sections.

2.4. Network Measures

2.4.1. Degree and Degree Centrality

For an undirected, unweighted network the degree k_i of node i is the number of neighbors of that node,

$$k_i = \sum_{j=1}^{N} A_{ij} \qquad (8)$$

where A_{ij} is the adjacency matrix and N is the number of nodes in the network.

To make degree comparable across networks of different sizes, we use the normalized degree centrality (Equation 9).

$$C_D(i) = \frac{k_i}{N - 1} \qquad (9)$$

so that $0 \leq C_D(i) \leq 1$. Nodes with high degree centrality are strongly connected to many other nodes and represent locations whose rainfall regime is similar to a large fraction of the zone.

Degree based metrics are widely used in complex networks and climate networks to highlight hubs and densely connected regions (Newman, 2010; Donges et al., 2009a).

2.4.2. Betweenness centrality

Betweenness centrality identifies nodes that lie on many shortest paths between other nodes and therefore act as connectors or bridges between different parts of the network (Freeman, 1977). For node i, betweenness centrality (Equation 10) is defined as

$$C_B(i) = \sum_{\substack{s,t=1 \\ s\neq i, t\neq i, s\neq t}}^{N} \frac{\sigma_{st}(i)}{\sigma_{st}} \qquad (10)$$

where σ_{st} is the number of shortest paths between nodes s and t and $\sigma_{st}(i)$ is the number of those paths that pass through node i.

Exact computation of C_B for large graphs can be expensive. We therefore use the implementation in NetworkX (Hagberg et al., 2008), which approximates betweenness centrality by sampling a fixed number k of source nodes when computing shortest paths (Brandes, 2001). We set $k = 150$ for all zones, which is less than the number of nodes but sufficient to stabilise the ranking of high-betweenness nodes. This approximation greatly reduces computational cost while preserving the relative ranking of nodes, which is the main quantity of interest in our interpretation of transition regions and connectors.

2.4.3. Community detection and modularity

To identify groups of nodes with internally similar rainfall regimes, we apply a modularity based community detection algorithm (Equation 10). Communities are subsets of nodes that are more densely connected to each other than to the rest of the network. Given a partition of the nodes into communities, modularity Q is

$$Q = \frac{1}{2E} \sum_{i=1}^{N} \sum_{j=1}^{N} (A_{ij} - \frac{k_i k_j}{2E})\, \delta(c_i, c_j), \qquad (11)$$

where E is the number of edges, k_i and k_j are the degrees of nodes i and j, c_i is the community index of node i, and $\delta(c_i, c_j)$ equals 1 when $c_i = c_j$ and 0 otherwise (Newman & Girvan, 2004). High values of Q indicate that the partition captures strong internal connectivity and weak external connectivity. We use the greedy modularity optimization algorithm of Clauset et al., (2004), as implemented in NetworkX (Hagberg et al., 2008). This algorithm iteratively merges

communities in a hierarchical fashion in order to approximately maximize Q, and is efficient for networks with up to tens of thousands of nodes, which fits the present application.

To interpret the physical meaning of communities, we compute for each community c in zone z the mean monthly precipitation profile

$$\bar{P}_{z,c}^{(m)} = \frac{1}{N_{z,c}} \sum_{i \in C_{z,c}} P_i^{(m)}, m = 1, \dots, 12, \qquad (12)$$

where $C_{z,c}$ is the set of nodes in community c, $N_{z,c} = | C_{z,c} |$, and $P_i^{(m)}$ is the precipitation at node i in month m. Plotting $\bar{P}_{z,c}^{(m)}$ for all communities in a zone reveals whether the communities are primarily distinguished by differences in annual totals, in the timing of the rainy season, or in a combination of both.

3. Results

3.1. Annual Precipitation

Annual precipitation over Saudi Arabia exhibits a pronounced spatial gradient structured into five classes (Figure 2). The driest class (4-50 mm yr^{-1}) is concentrated over the north-western interior, indicating extensive hyper-arid conditions. The next class (50-100 mm yr^{-1}) covers most of the central and eastern interior and represents the dominant dry background regime. The intermediate totals (100-150 mm and 150-200 mm yr^{-1}) form two broad transition bands that arc from the southwest toward the north-central sector, reflecting a gradual shift from hyper-arid to more humid conditions. The wettest class (200-299 mm yr^{-1}) occurs in two distinct cores: one along the southwestern highlands and a second smaller core in the north-eastern part of the country near the Gulf coast. These two wet clusters indicate where orographic and frontal systems most effectively enhance rainfall compared with the surrounding interior.

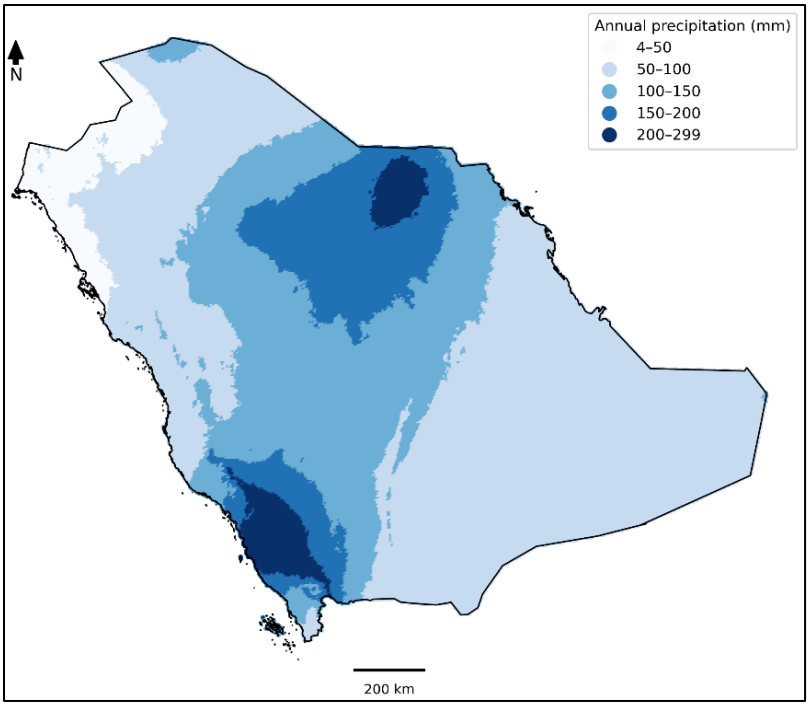

Figure 2. Annual precipitation over Saudi Arabia derived from WorldClim.

3.2. Precipitation Zones

The precipitation zoning map shows that Saudi Arabia is dominated by hyber-arid and arid conditions, with only limited pockets of relatively high rainfall (Figure 3). Hyper-arid conditions (Zone 1, 4-75 mm yr^{-1}) occur mainly along the northern and north-western deserts, across much of the eastern and south-eastern interior, and within large parts of the southern Rubʿ al-Khali. A broad arid belt (Zone 2, 75-150 mm yr^{-1}) occupies most of the central interior from south-west to north-east, forming a continuous transition between the driest margins and the wetter highlands. Wet conditions (Zone 3, ≥150 mm yr^{-1}) are restricted to two compact clusters: one along the south-western escarpment adjacent to the Red Sea and another over an area in the north-central part of the country. In terms of grid-cell counts, Zones 1, 2, and 3 account for approximately 31 %, 52 %, and 17 % of the study domain, respectively, underscoring the limited spatial extent of the wetter environments.

This tripartite classification into hyper-arid, arid, and semi-arid zones provides a physically meaningful basis for the subsequent network analysis. Treating each zone as a separate hydro-climatic regime avoids mixing fundamentally different environments in a single graph and allows the networks to capture internal connectivity within comparable rainfall conditions. From a water-resources perspective, the zoning highlights where chronic water scarcity is structurally embedded in the climate, where both drought and flash-flood risk must be considered together along the arid transition belt, and where the country's limited high-rainfall areas are concentrated. These spatial

contrasts frame the interpretation of degree centrality, betweenness, and community structure in the following sections.

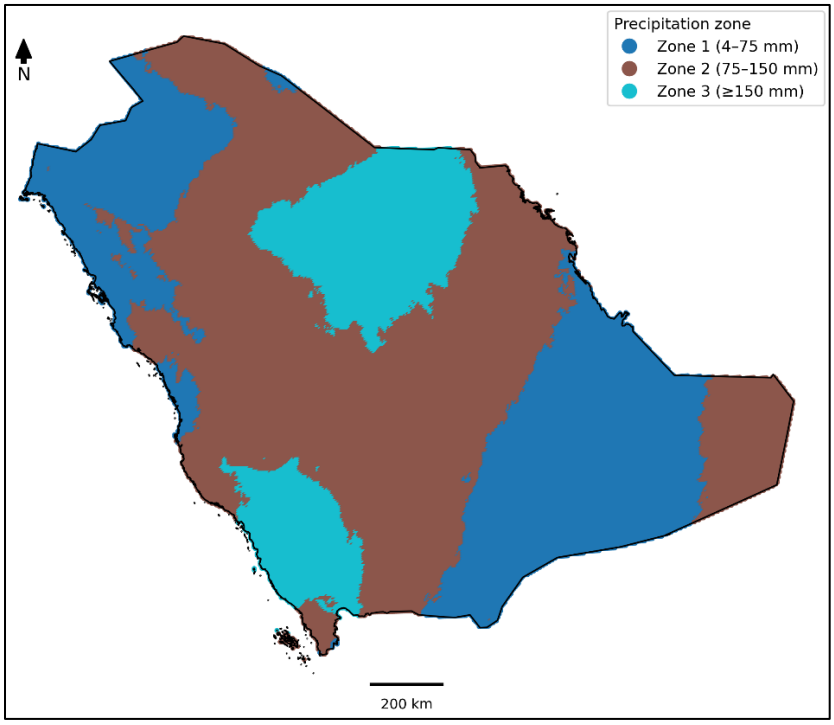

Figure 3. Precipitation zones across Saudi Arabia.

3.3. Sampling Design Analysis

Figure 4 illustrates how the WorldClim grid was reduced from the full set of precipitation points to the subset used in the network analysis. The light grey symbols represent all land grid cells at 2.5-minute resolution over Saudi Arabia (98,719 nodes), whereas the red points show the stratified sample of 7,148 nodes. The sampled nodes are distributed across the entire country, ensuring the sample includes points from all major regions that had data in the full grid. This confirms that the sampling procedure preserves the spatial footprint of the original dataset.

Sampling density is somewhat higher in the south-western highlands and in parts of the central north, where annual rainfall is larger and spatial gradients are sharper. This pattern is consistent with the stratified design based on annual precipitation bins, which allocates similar numbers of nodes to each rainfall class so that the wet and transition regimes are adequately represented even though they occupy smaller areas than the dry regions. Figure 4 therefore provides a visual justification for the network analysis, demonstrating that the reduced dataset maintains both geographic coverage and rainfall-regime diversity while keeping the number of nodes at a computationally tractable level.

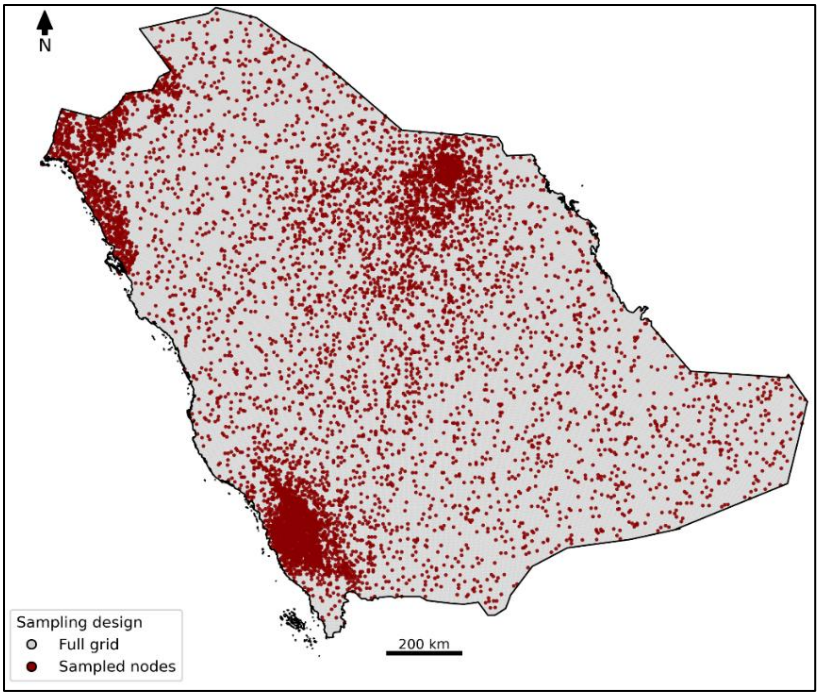

Figure 4. Full WorldClim precipitation grid (grey) and stratified sample used for network construction (red).

3.4. Degree & Betweenness Centrality Analysis

Figure 5 summarises the distribution of degree and betweenness centrality for all sampled nodes in the three precipitation zones for the reference threshold $r = 0.80$ and $k = 150$ source nodes in the betweenness calculation. Degree centrality is generally high in all zones, which is expected given that edges are only drawn between nodes with strong correlation. Zone 2, representing the arid central belt, has the highest median degree and the widest upper range, with many nodes between about 0.4 and 0.6 and some approaching 0.8. This indicates that within Zone 2 a large fraction of grid cells share very similar seasonal precipitation cycles and form a dense, internally coherent rainfall regime.

Zones 1 and 3 exhibit slightly lower median degree values and somewhat narrower upper ranges. In both zones many nodes remain well connected, but there is a larger proportion of nodes with modest degree centrality compared with Zone 2. This suggests that the hyper-arid and wet zones contain more locations whose precipitation regime is distinctive within the zone and therefore less similar to a large number of neighbours, whereas the arid interior behaves more like a single, spatially coherent field.

The right-hand panel of Figure 5 shows betweenness centrality on a logarithmic scale. In all three zones the distribution is highly skewed: most nodes have values around 10^{-4} or lower, while only a small subset reach values of order 10^{-3}–10^{-2}. This pattern indicates that the climate networks are dominated by local connections; only a minority of nodes act as internal “bridges”

that lie on many shortest paths between other nodes within the same zone. Differences between zones are modest: Zone 1 shows slightly higher extreme values, while Zone 2 has the lowest mean betweenness, consistent with a fairly homogeneous arid regime in which there are fewer indispensable "transit nodes". Because networks were constructed separately for each precipitation zone, these betweenness values describe connectivity within each hydro-climatic regime rather than links between zones.

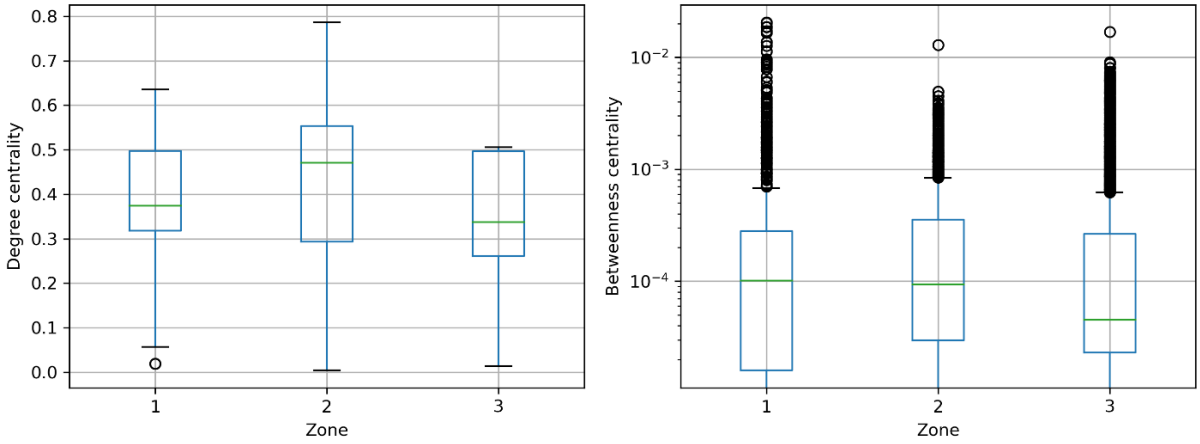

Figure 5. Distributions of degree centrality and betweenness centrality (log scale) for all sampled nodes in the three precipitation zones

3.5. Degree Centrality and Community Structure

Figure 6 shows how the precipitation network is organised within each of the three precipitation zones for the reference threshold $r = 0.80$. In all panels, degree centrality measures the fraction of nodes inside a zone that are strongly correlated with a given node, while the community maps display the groups identified by modularity optimization.

Zone 1 (4–75 mm yr^{-1})

In the hyper-arid zone, the highest degree values occur mainly along the north-western Red Sea margin and in the south-eastern fringe, whereas the deep interior of the Empty Quarter and the northern desert show much lower connectivity. This indicates that coastal and peripheral parts of Zone 1 share a common pattern of monthly precipitation seasonal cycles with many other grid cells, while the interior desert is more weakly linked to the rest of the zone. The community map shows a clear separation between a western community and an eastern community, with a relatively diffuse transition in central Saudi Arabia. Even within very dry conditions, the network therefore distinguishes at least two large sub-regions in which dry and wet months tend to occur in phase.

Zone 2 (75–150 mm yr^{-1})

The arid belt displays a different structure. Degree centrality is highest along a broad corridor

that connects the south-western highlands with the central plateau, which points to a large area where monthly precipitation variability is highly coherent. Degree values decrease toward the far north-west and the eastern margins of Zone 2, suggesting that rainfall there is more localised or influenced by additional processes. Community detection splits Zone 2 into three large clusters: a western-south-western community aligned with the escarpment and adjacent plateau, a central community, and an eastern community extending toward the Gulf region. These clusters represent distinct arid regimes that share a common seasonal cycle internally but differ in how strongly they are connected to the rest of the zone.

Zone 3 (≥150 mm yr^{-1})

In the wettest zone, nodes are concentrated in two separated clusters: the south-western mountains and a smaller high-rainfall region in the central north. Within each cluster, degree centrality is generally high, indicating dense connectivity and strong synchrony of monthly rainfall among neighbouring cells. The community map almost perfectly separates these two clusters, with very little spatial overlap. From the perspective of monthly variability, the south-western orographic region and the northern high-rainfall region therefore behave as two largely independent regimes, even though they both exceed 150 mm yr^{-1} in annual totals.

These maps show that the precipitation networks within the three macro-zones are far from random. They organize into a small number of spatially coherent communities with systematic contrasts in degree centrality, which supports the idea that rainfall over Saudi Arabia can be represented by a limited set of connected regimes rather than many isolated grid cells.

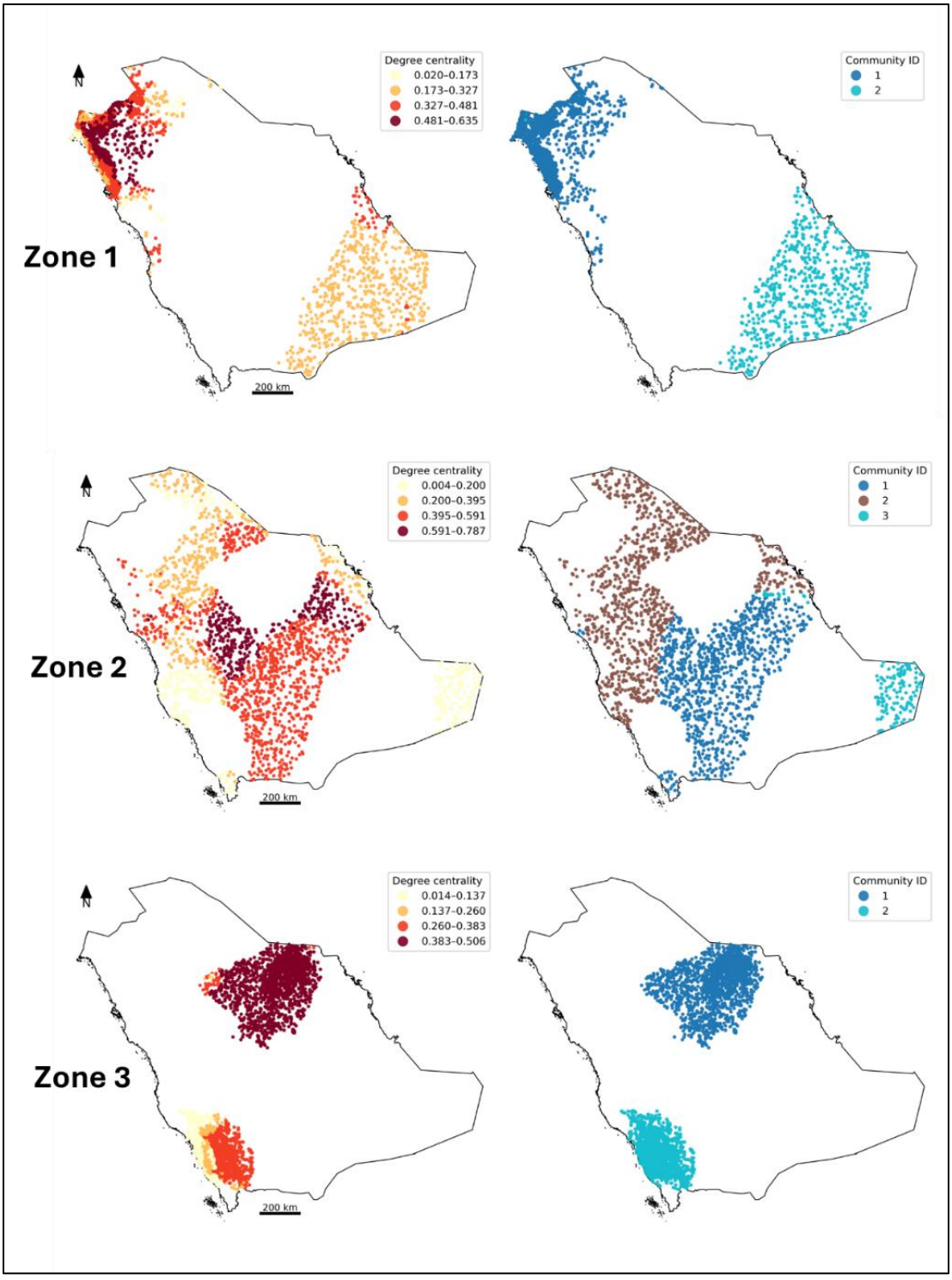

Figure 6. Spatial patterns of degree centrality and community structure for the three precipitation zones

3.6. Seasonal Precipitation Regimes by Community

Figure 7 presents the mean monthly precipitation profiles of each community in the three zones and clarifies the climatic meaning of the network-derived communities.

Zone 1 (4–75 mm yr^{-1})

Both communities are very dry, with rainfall concentrated in late winter and early spring. Community 2 has a sharp peak in March and consistently higher values, while Community 1 receives roughly half as much rainfall and exhibits a broader but weaker cool-season maximum. Combined with the maps, this implies that the coastal and fringe parts of Zone 1 experience more intense and more sharply timed winter storms, whereas the interior desert is drier and responds more weakly, with diffuse and sporadic events.

Zone 2 (75–150 mm yr^{-1})

All three communities share a spring-dominated regime with a pronounced March maximum, but they differ in intensity and in the width of the rainy season. Community 1 has the highest March peak and very limited rainfall outside January-April, indicating a strongly winter-dominated pattern characteristic of the central plateau. Community 2 shows a similar peak but maintains more rainfall into April and the early winter months, giving a broader cool-season window. Community 3 is comparatively wetter in January-February and declines more quickly after March, consistent with locations that are more exposed to early winter disturbances and less to late spring convection. The network has thus separated the arid belt into three variants of the same basic pattern that differ in how concentrated the rainy season is.

Zone 3 (≥150 mm yr^{-1})

Seasonal contrasts are strongest in Zone 3. Community 1 shows a marked winter and early spring maximum, with high precipitation from January to April, almost no rainfall in June-August, and a recovery in autumn. This behaviour matches a Mediterranean-type regime driven primarily by winter frontal systems, which characterizes the northern high-rainfall area. Community 2 maintains substantial rainfall from May through September and exhibits a secondary late-summer maximum, consistent with monsoon and Red Sea influences over the south-western highlands. Here the network clearly separates two physically distinct regimes that would be difficult to distinguish using only annual totals.

Overall, the monthly profiles confirm that communities identified by the network are not arbitrary geospatial clusters. Within each zone, nodes assigned to the same community share both the timing and relative magnitude of rainfall through the year, whereas differences between communities correspond to meaningful shifts in when and how precipitation occurs over Saudi Arabia.

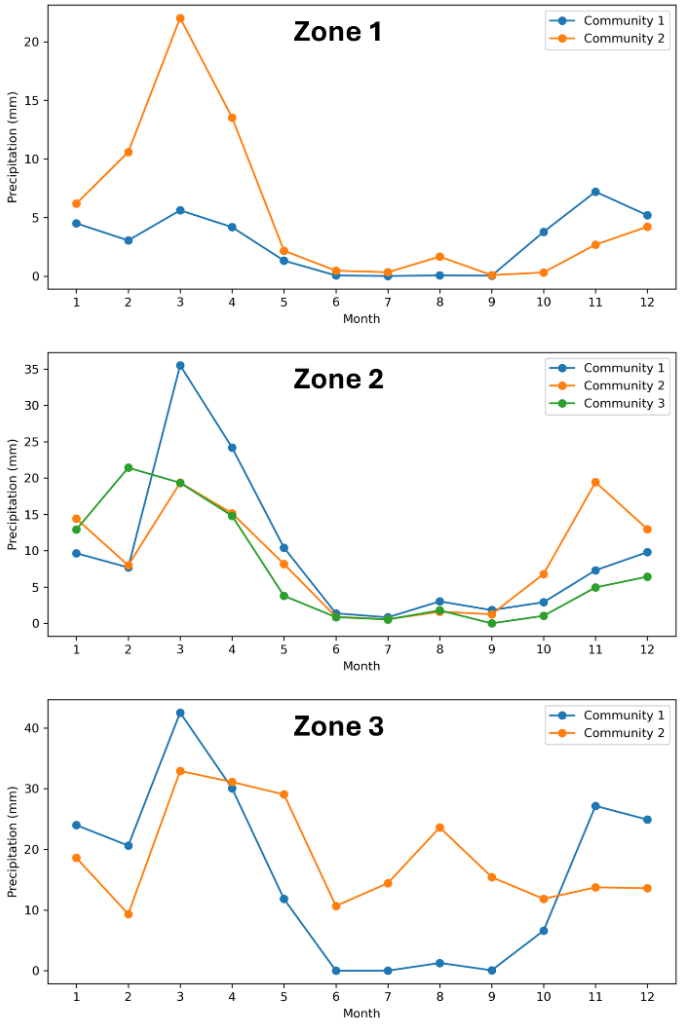

Figure 7. The mean monthly precipitation regime for the communities identified inside each zone.

3.7. Summary Community Stats

Table 1. Summary of community characteristics

Zone	Community ID	No. of nodes	Mean annual	Mean degree	Min degree	Max degree	Mean betweenness	Max betweenness
1	1	1275	35	0.4339	0.0196	0.6349	0.0004	0.0206
	2	613	64	0.3103	0.1971	0.3720	0.0006	0.0205
2	1	984	114	0.5376	0.0043	0.7490	0.0003	0.0049
	2	952	108	0.3402	0.0255	0.7865	0.0004	0.0129
	3	145	87	0.1939	0.0856	0.7697	0.0003	0.0032
3	1	1608	189	0.4810	0.0906	0.5057	0.0003	0.0169
	2	1571	224	0.2150	0.0142	0.3461	0.0006	0.0090

Table 1 summarizes the main properties of the communities identified at the reference threshold $r = 0.80$. For each community it reports the number of nodes, mean annual precipitation, mean and range of degree centrality, and mean and maximum betweenness centrality. Together with the maps and monthly profiles, these statistics clarify how rainfall amount and network role co-vary within each macro-zone.

Zone 1 (4–75 mm yr^{-1})

Zone 1 separates into two communities with distinct hydro-climatic behaviour. Community 1 (1,275 nodes) is drier on average, with about 35 mm yr^{-1}, yet it has the highest mean degree centrality in the zone (≈ 0.43, maximum ≈ 0.63). These nodes are strongly connected to many other nodes in Zone 1, which indicates a highly coherent hyper-arid core where dry and relatively wet months tend to occur in phase across wide areas. Mean betweenness is modest, so most of these nodes sit inside the main cluster rather than acting as bridges. Community 2 (613 nodes) is considerably wetter (≈ 64 mm yr^{-1}) but less connected (mean degree ≈ 0.31). It represents a more localised regime located mainly along the desert fringe. Its slightly higher mean betweenness suggests that some nodes help connect the hyper-arid core to wetter margins. Overall, Zone 1 consists of a very dry but network-coherent interior and a wetter, structurally more peripheral fringe.

Zone 2 (75–150 mm yr^{-1})

The arid belt is organized into three communities that form a gradient in both rainfall and connectivity. Community 1 (984 nodes) is the wettest group in Zone 2 (mean ≈ 115 mm yr^{-1}) and also the most connected (mean degree ≈ 0.54). These locations share strong correlations with more than half of the other nodes, which confirms the presence of a large, internally coherent arid regime. Community 2 (952 nodes) has slightly lower annual rainfall (≈ 109 mm yr^{-1}) and a reduced mean degree (≈ 0.34). It still forms a substantial arid regime, but its weaker connectivity and higher maximum betweenness (≈ 0.013) indicate that a subset of nodes plays an important bridge role between different parts of the Zone 2 network. Community 3 (145 nodes) is the smallest and driest arid group (≈ 88 mm yr^{-1}) with the lowest mean degree (≈ 0.19). It corresponds to a marginal regime where rainfall patterns are less tightly synchronized with the rest of the zone, although a few nodes still provide non-negligible links to the main arid core.

Zone 3 (≥150 mm yr^{-1})

The wet zone contains two large communities that differ in both rainfall amount and network structure. Community 1 (1,608 nodes) has a mean annual precipitation of about 189 mm and relatively high connectivity (mean degree ≈ 0.48). It corresponds mainly to the northern wet region, where monthly precipitation anomalies are tightly synchronized across many nodes. Maximum betweenness (≈ 0.017) indicates that a small subset of locations acts as important connectors within the wet network. Community 2 (1,571 nodes) is the wettest group in the study (mean ≈ 224 mm yr^{-1}), but its mean degree is much lower (≈ 0.22) and its maximum degree is only about 0.35. This pattern suggests that rainfall in the south-western mountains is spatially more heterogeneous, with strong co-variability at short distances but weaker links to the rest of

Zone 3. Slightly higher average betweenness compared with Community 1 points to nodes that bridge small, locally coherent clusters. Together, these statistics reinforce the interpretation of Zone 3 as comprising a moderately wet but cohesive northern regime and a wetter, more fragmented orographic regime in the south-west.

3.8. Sensitivity Analysis

The sensitivity analysis repeated the network construction for correlation thresholds of 0.75, 0.80 and 0.85 in each zone (Figure 8). As expected, the number of edges declined monotonically with increasing threshold, since fewer pairs of nodes exceeded the stricter similarity criterion. For all three thresholds, Zone 3 consistently exhibited the densest network, followed by Zone 2 and then Zone 1, which is consistent with the higher spatial coherence of rainfall in wetter regions. Mean degree centrality also decreased with increasing threshold, while betweenness centrality showed a modest increase in its upper range, reflecting the fact that, in sparser graphs, a smaller set of nodes carries a larger share of the shortest paths.

Despite these changes in density and centrality magnitudes, the community structure remained remarkably stable. Across all thresholds, Zone 1 was partitioned into two communities, Zone 2 into three communities, and Zone 3 into two communities, with only minor shifts in community boundaries. The spatial patterns of the main communities and their associated monthly precipitation regimes were preserved. This robustness indicates that the identified rainfall communities are not an artefact of a particular correlation threshold but instead represent persistent structural features of the precipitation field. On this basis, using $r = 0.80$ as the reference threshold in the main analysis provides a reasonable compromise between network density and selectivity for strong similarities.

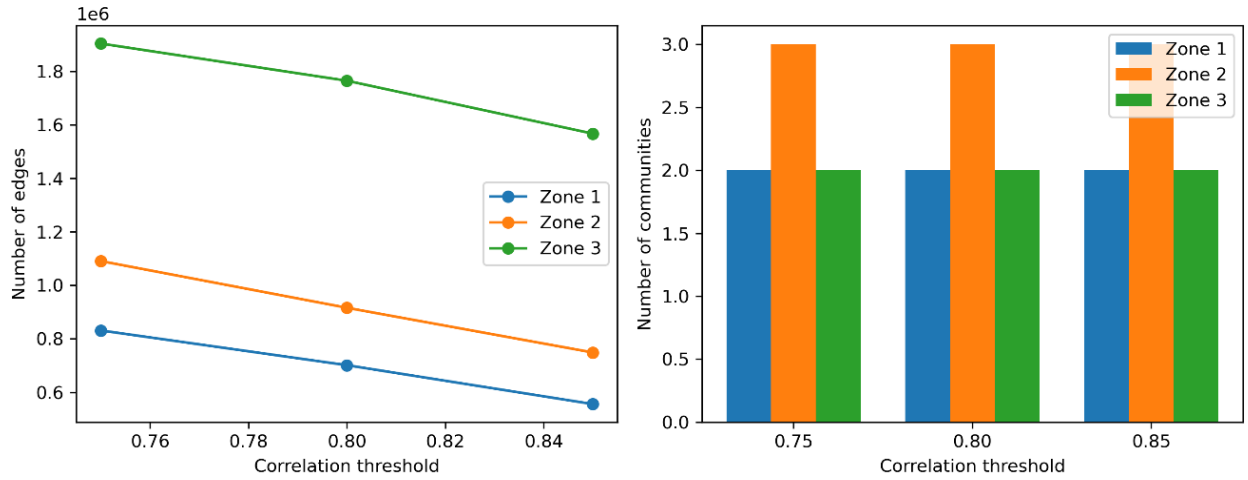

Figure 8. Sensitivity of network structure to the correlation threshold

4. Discussion

The climate network analysis provides an integrated view of precipitation variability across Saudi Arabia by linking spatial rainfall patterns to large scale circulation and topography. The WorldClim gradient from hyper arid northern and inland deserts to semi-arid southwestern highlands is consistent with the three dominant systems that modulate rainfall over the Arabian Peninsula: Mediterranean winter fronts affecting the northwest and north central regions, Red Sea Trough related convection over western and central sectors, and orographic uplift along the Asir and Hejaz ranges that enhances summer and transition season rainfall (Abdullah & Al-Mazroui, 1998; Almazroui et al., 2012; Hasanean & Al-Mazroui, 2015; Luong et al., 2025). These circulation driven contrasts agree with recent analyses of temperature, precipitation, drought and visibility patterns over Saudi Arabia (Alhathloul et al., 2024; Alhathloul & Alnahit, 2024) and support the division into hyper arid, arid and wet zones as a compact hydro climatic framework for network-based diagnostics (AlSarmi & Washington, 2014; Wang et al., 2025).

Network metrics reveal pronounced structural differences among the three zones. The arid zone (Zone 2) has the highest degree centrality, indicating a large, internally coherent rainfall domain and strong spatial synchrony of winter precipitation across the central plateau (AlSarmi & Washington, 2011; Hasanean & Al-Mazroui, 2015; Luong et al., 2025). In contrast, the hyper arid zone (Zone 1) and the wet zone (Zone 3) show lower mean degree and higher variability, consistent with localized and intermittent rainfall in the northern deserts and strong small-scale heterogeneity in the southwestern mountains (Abdullah & Al-Mazroui, 1998; Almazroui et al., 2012; Wang et al., 2025). Betweenness centrality highlights transition areas that act as climatic bridges: high betweenness nodes along the western escarpment, the northern fringe of the Empty Quarter and corridors within Zone 2 lie on disproportionately many shortest paths, similar to bridge regions identified in earlier climate networks (Donges et al., 2009a; Luong et al., 2025). Such nodes mark overlap zones where multiple mechanisms shape seasonal precipitation and may be sensitive to shifts in synoptic patterns and changes in Red Sea warming.

Community detection further clarifies the spatial organization of rainfall regimes. In each zone only a small number of communities emerge, and their mean monthly cycles correspond to distinct seasonal regimes that agree with earlier regionalizations based on synoptic typing and empirical orthogonal functions (Almazroui et al., 2012; Hasanean & Al-Mazroui, 2015; Luong et al., 2025). In Zone 3 the separation between a northern Mediterranean frontal regime and a southwestern orographic monsoonal regime is consistent with documented contrasts between frontal and orographic rainfall in western and southwestern Saudi Arabia (Abdullah & Al-Mazroui, 1998; AlSarmi & Washington, 2014). The persistence of these communities across correlation thresholds from 0.75 to 0.85 shows that they are robust features of the precipitation field rather than artifacts of parameter choice, in line with work demonstrating that stable communities often mirror long standing climatic divisions constrained by dynamics and topography (Donges et al., 2009b; Tantet & Dijkstra, 2014).

The stratified sampling design guarantees that dry, semi-arid and transition regimes are all represented while reducing the full WorldClim grid to a tractable node set that preserves major spatial gradients. This increases confidence that the community and centrality patterns reflect genuine climatic organization rather than uneven data density and provides a concise climate background for drought and flood risk assessment, hydrologic modelling and decision support. Strong connectivity in the arid interior suggests that regional drought monitoring and seasonal forecasting can exploit the coherent response of large areas to circulation anomalies, whereas fragmented connectivity in the southwestern wet zone points to the need for higher resolution hydrological and flood forecasting tools and denser observation networks in mountainous catchments (Mishra & Singh, 2010; Hasanean & Al-Mazroui, 2015; Wang et al., 2025; Alhathloul & Alnahit, 2024). The identified regimes can also be coupled with flood exposure, vulnerability and accessibility analyses to support integrated risk management and web-based decision support systems (Alabbad & Demir, 2022; Alabbad et al., 2022). The main limitation of the present analysis is its reliance on a single long term monthly climatology and a correlation-based similarity measure, which may not fully capture event scale extremes or interannual variability and should be considered when applying the identified regimes in local hydrologic and impact-oriented studies.

5. Conclusion

This study applied a climate network approach to characterize long term precipitation regimes in Saudi Arabia using WorldClim v2.1 monthly climatology. We combined a simple zonation based on annual rainfall, a stratified sampling scheme, and correlation based networks (with degree, betweenness, and modularity analysis) constructed separately for each zone. The three annual rainfall zones reproduced the major hydro climatic gradients across the country and provided a natural framework for analysis. The stratified sampling design reduced the full grid of almost 100,000 cells to a manageable set of 7,148 nodes while preserving the spatial footprint and the distribution of annual precipitation. Within each zone, the resulting networks were highly connected and contained only two or three communities, which corresponded to coherent seasonal rainfall regimes. Degree centrality highlighted locations whose monthly cycle was representative of large parts of a zone, whereas betweenness centrality pinpointed transition belts and fringe areas that act as connectors between regimes. Sensitivity tests across correlation thresholds showed that these communities and centrality patterns are structurally robust.

The proposed framework offers a compact and reproducible way to summarize complex spatial patterns of rainfall in data scarce arid regions. By reducing the precipitation field to a small number of connected regimes with clear geographic signatures, it provides information that can be linked directly to hydrologic modelling, flood and drought risk assessment, agricultural planning, climate change adaptation planning and ecosystem management. Future work could extend the analysis to time varying networks based on interannual anomalies or extreme events, incorporate additional variables such as temperature or circulation indices to study

teleconnections, or use higher resolution regional climate simulations and terrain data to refine orographic effects. Although the present results rely on a single gridded product (WorldClim) and long-term average climatology, the methodology is general and transferable and can support ongoing efforts to understand and manage water resources under a changing climate in Saudi Arabia and similar environments.

6. References

1. Abdullah, M. A., & Al-Mazroui, M. A. (1998). Climatological study of the southwestern region of Saudi Arabia: I. Rainfall analysis. *Climate Research, 9*(3), 213–223.
2. Alabbad, Y., Mount, J., Campbell, A. M., & Demir, I. (2021). Assessment of transportation system disruption and accessibility to critical amenities during flooding: Iowa case study. *Science of the total environment*, *793*, 148476.
3. Alabbad, Y., & Demir, I. (2022). Comprehensive flood vulnerability analysis in urban communities: Iowa case study. *International journal of disaster risk reduction*, *74*, 102955.
4. Alabbad, Y., Yildirim, E., & Demir, I. (2022). Flood mitigation data analytics and decision support framework: Iowa Middle Cedar Watershed case study. *Science of The Total Environment*, *814*, 152768.
5. Alhathloul, S. H., & Alnahit, A. O. (2024). Long-Term Spatiotemporal Variation of Drought Patterns over Saudi Arabia. *Water*, *17*(1), 72.
6. Alhathloul, S. H., Khan, A. A., & Mishra, A. K. (2024). Temporal variability of temperature, precipitation, drought, and their potential influence on horizontal visibility over Saudi Arabia. *Theoretical and Applied Climatology*, *155*(6), 4621-4639.
7. AlSarmi, S. H., & Washington, R. (2014). Changes in climate extremes in the Arabian Peninsula: analysis of daily data. *Int. J. Climatol*, *34*(5), 1329-1345.
8. Almazroui, M. (2011). Calibration of TRMM rainfall climatology over Saudi Arabia during 1998–2009. *Atmospheric Research, 99*(3–4), 400–414.
9. Almazroui, M. (2019). Climate extremes over the Arabian Peninsula using RegCM4 for present conditions forced by several CMIP5 models. *Atmosphere*, *10*(11), 675.
10. Almazroui, M., & Hasanean, H. M. (2020). Saudi Arabia's summer surface air temperature and its association with circulation patterns. *Int. J. Climatol*, *40*, 5727-5743.
11. Almazroui, M., Islam, M. N., Jones, P. D., Athar, H., & Rahman, M. A. (2012). Recent climate change in the Arabian Peninsula: Seasonal rainfall and temperature climatology of Saudi Arabia for 1979–2009. *Atmospheric Research, 111*, 29-45.
12. Almazroui, M., Saeed, S., Islam, M. N., Alkhalaf, A. K., & Dambul, R. (2017). Assessing the robustness and uncertainties of projected changes in temperature and precipitation in AR5 global climate models over the Arabian Peninsula. *Atmospheric Research, 194*, 202–213.
13. Bahrawi, J. A. (2018). Rainfall distribution and its characteristics in Makkah Al-Mukarramah region, Saudi Arabia. *Applied Ecology & Environmental Research*, *16*(4).
14. Boers, N., Bookhagen, B., Marwan, N., Kurths, J., & Marengo, J. (2013). Complex networks identify spatial patterns of extreme rainfall events of the South American Monsoon System. *Geophysical Research Letters, 40*(16), 4386–4392.
15. Boers, N., Goswami, B., Rheinwalt, A., Bookhagen, B., Hoskins, B., & Kurths, J. (2019). Complex networks reveal global pattern of extreme-rainfall teleconnections. *Nature, 566*(7744), 373–377.

16. Brandes, U. (2001). A faster algorithm for betweenness centrality. *Journal of Mathematical Sociology, 25*(2), 163–177.
17. Cerasoli, F., D'Alessandro, P., & Biondi, M. (2022). Worldclim 2.1 versus Worldclim 1.4: Climatic niche and grid resolution affect between-version mismatches in habitat suitability models predictions across Europe. *Ecology and evolution*, *12*(2), e8430.
18. Clauset, A., Newman, M. E., & Moore, C. (2004). Finding community structure in very large networks. *Physical Review E—Statistical, Nonlinear, and Soft Matter Physics*, *70*(6), 066111.
19. Cochran, W.G. (1977) Sampling Techniques. 3rd Edition, John Wiley & Sons, New York.
20. Dastorani, M. T., & Poormohammadi, S. (2016). Mapping of climatic parameters under climate change impacts in Iran. Hydrological Sciences Journal, 61(14), 2552-2566.
21. Deza, M. M., & Deza, E. (2009). Encyclopedia of distances. In *Encyclopedia of distances* (pp. 1-583). Berlin, Heidelberg: Springer Berlin Heidelberg.
22. Donges, J. F., Zou, Y., Marwan, N., & Kurths, J. (2009a). Complex networks in climate dynamics: Comparing linear and nonlinear network construction methods. *The European Physical Journal Special Topics, 174*(1), 157–179.
23. Donges, J. F., Zou, Y., Marwan, N., & Kurths, J. (2009b). The backbone of the climate network. *Europhysics Letters, 87*(4), 48007.
24. Fick, S. E., & Hijmans, R. J. (2017). WorldClim 2: New 1-km spatial resolution climate surfaces for global land areas. *International Journal of Climatology, 37*(12), 4302–4315.
25. Freeman, L. C. (1977). A set of measures of centrality based on betweenness. *Sociometry*, 35-41.
26. Gratzfeld, J. (2003). *Extractive industries in arid and semi-arid zones: Environmental planning and management*. IUCN.
27. Haas, M., Goswami, B., & von Luxburg, U. (2023). Pitfalls of climate network construction—a statistical perspective. *Journal of Climate*, *36*(10), 3321-3342.
28. Hagberg, A., Swart, P. J., & Schult, D. A. (2008). *Exploring network structure, dynamics, and function using NetworkX* (No. LA-UR-08-05495; LA-UR-08-5495). Los Alamos National Laboratory (LANL), Los Alamos, NM (United States).
29. Hasanean, H. M., & Almazroui, M. (2015). Rainfall: Features and variations over Saudi Arabia, a review. *Climate, 3*(3), 578–626.
30. Hereher, M. E. (2016). Recent trends of temperature and precipitation proxies in Saudi Arabia: implications for climate change. *Arabian Journal of Geosciences*, *9*(11), 575.
31. Luong, T. M., Dasari, H. P., Attada, R., Chang, H. I., Risanto, C. B., Castro, C. L., ... & Hoteit, I. (2025). Rainfall climatology and predictability over the Kingdom of Saudi Arabia at subseasonal scale. *Quarterly Journal of the Royal Meteorological Society*, e5015.
32. Jahn, S., Gaythorpe, K. A., Wainwright, C. M., & Ferguson, N. M. (2025). Evaluation of the performance and utility of global gridded precipitation products for health applications and impact assessments in South America. *GeoHealth*, *9*(6), e2024GH001260.
33. Lohr, S. L. (2021). *Sampling: design and analysis*. Chapman and Hall/CRC.
34. Lutz, A. F., Immerzeel, W. W., Kraaijenbrink, P. D., Shrestha, A. B., & Bierkens, M. F. (2016). Climate change impacts on the upper Indus hydrology: sources, shifts and extremes. *PloS one*, *11*(11), e0165630.
35. Marwan, N., Donges, J. F., Zou, Y., Donner, R. V., & Kurths, J. (2009). Complex network approach for recurrence analysis of time series. *Physics Letters A, 373*(46), 4246–4254.

36. Mankin, K. R., Mehan, S., Green, T. R., & Barnard, D. M. (2025). Review of gridded climate products and their use in hydrological analyses reveals overlaps, gaps, and the need for a more objective approach to selecting model forcing datasets. *Hydrology and Earth System Sciences*, *29*(1), 85-108.
37. Middleton, N., & Thomas, D. (1997). *World atlas of desertification* (2nd ed.). Arnold / UNEP.
38. Mishra, A. K., & Singh, V. P. (2010). A review of drought concepts. *Journal of hydrology*, *391*(1-2), 202-216.
39. Nelli, N. R., Francis, D., Fonseca, R., Abida, R., Weston, M., Wehbe, Y., & Al Hosary, T. (2021). The atmospheric controls of extreme convective events over the southern Arabian Peninsula during the spring season. *Atmospheric Research*, *262*, 105788.
40. Newman, M. E. J. (2010). *Networks: An introduction*. Oxford University Press.
41. Newman, M. E. J., & Girvan, M. (2004). Finding and evaluating community structure in networks. *Physical Review E, 69*(2), 026113.
42. Scarsoglio, S., Laio, F., & Ridolfi, L. (2013). Climate dynamics: A network-based approach for the analysis of global precipitation. *PLoS ONE, 8*(8), e71129.
43. Steinhaeuser, K., Chawla, N. V., & Ganguly, A. R. (2009, June). An exploration of climate data using complex networks. In *Proceedings of the Third International Workshop on Knowledge Discovery from Sensor Data* (pp. 23-31).
44. Stolbova, V., Martin, P., Bookhagen, B., Marwan, N., & Kurths, J. (2014). Topology and seasonal evolution of the network of extreme precipitation over the Indian subcontinent and Sri Lanka. *Nonlinear Processes in Geophysics, 21*(4), 901–917.
45. Tantet, A., & Dijkstra, H. A. (2014). An interaction network perspective on the relation between patterns of sea surface temperature variability and global mean surface temperature. *Earth System Dynamics*, *5*(1), 1-14.
46. Tsonis, A. A., & Roebber, P. J. (2004). The architecture of the climate network. *Physica A: Statistical Mechanics and its Applications*, *333*, 497-504.
47. UNEP. (1997). *World atlas of desertification* (2nd ed.). United Nations Environment Programme.
48. Wang, X., Alharbi, R. S., Baez-Villanueva, O. M., Green, A., McCabe, M. F., Wada, Y., ... & Beck, H. E. (2025). Saudi Rainfall (SaRa): hourly 0.1° gridded rainfall (1979–present) for Saudi Arabia via machine learning fusion of satellite and model data. *Hydrology and Earth System Sciences*, *29*(19), 4983-5003.
49. Wolf, F., & Donner, R. V. (2021). Spatial organization of connectivity in functional climate networks describing event synchrony of heavy precipitation. *The European Physical Journal Special Topics*, *230*(14), 3045-3063.
50. Yamasaki, K., Gozolchiani, A., & Havlin, S. (2008). Climate networks around the globe are significantly affected by El Nino. *Physical review letters*, *100*(22), 228501.
51. Zomer, R. J., Trabucco, A., Bossio, D. A., & Verchot, L. V. (2008). Climate change mitigation: A spatial analysis of global land suitability for clean development mechanism afforestation and reforestation. *Agriculture, ecosystems & environment*, *126*(1-2), 67-80.
52. Zou, Y., Donner, R. V., Marwan, N., Donges, J. F., & Kurths, J. (2019). Complex network approaches to nonlinear time series analysis. *Physics Reports*, *787*, 1-97.